J Nanopart Res (2008) 10:1251–1262
DOI 10.1007/s11051-007-9349-9

RESEARCH PAPER

Er:YAB nanoparticles and vitreous thin films by the polymeric precursor method

Lauro J. Q. Maia · Alain Ibanez · Luc Ortega · Valmor R. Mastelaro · Antonio C. Hernandes

Received: 27 August 2006 / Accepted: 10 December 2007 / Published online: 5 February 2008

Abstract The synthesis of $Y_{0.9}Er_{0.1}Al_3(BO_3)_4$ crystalline powders and vitreous thin films were studied. Precursor solutions were obtained using a modified polymeric precursor method using D-sorbitol as complexant agent. The chemical reactions were described. $Y_{0.9}Er_{0.1}Al_3(BO_3)_4$ composition presents good thermal stability with regard to crystallization. The $Y_{0.9}Er_{0.1}Al_3(BO_3)_4$ crystallized phase can be obtained at 1,150 °C, in agreement with other authors. Crack- and porosity-free films were obtained with very small grain size and low RMS roughness. The films thickness revealed to be linearly dependent on precursor solution viscosity, being the value of 25 mPa s useful to prepare high-quality amorphous multi-layers (up to ~ 800 nm) at 740 °C during 2 h onto silica substrates by spin coating with a gyrset technology.

Keywords Er:YAB · Nanopowder · Nanoparticles · Thin films · Polymeric precursor method · Thermal analysis · FEG · XRD · GIXRD · AFM

L. J. Q. Maia (✉) · V. R. Mastelaro · A. C. Hernandes
Grupo Crescimento de Cristais e Materiais Cerâmicos, Departamento de Fisica e Ciência dos Materiais, Instituto de Fisica de São Carlos, Universidade de São Paulo, Caixa Postal 369, 13560-970 Sao Carlos, SP, Brazil
e-mail: lauro@if.sc.usp.br

L. J. Q. Maia · A. Ibanez · L. Ortega
Laboratoire de Cristallographie CNRS associé à l'Université Joseph Fourier et à l'INPG, 25 Avenue des Martyrs, BP 166, 38042 Grenoble, France

Introduction

Optical properties of rare-earth ions incorporated to glassy hosts are of great interest in opto-electronic technology (Urquhart 1988). Rare-earth trivalent ions in some solid compounds emit light at characteristic wavelengths due to intra-4*f* or internal 4*f*–5*d* transitions. In the case of Er^{3+}, the emission at 1.54 μm corresponds to a dipole forbidden intra 4*f* transition $^4I_{13/2}$ to $^4I_{15/2}$, which coincides with the low-loss window of standard optical telecommunications silica fiber (Kik and Polman 1998).

In the last years, extraordinary progress has been achieved in the development of single-mode Er-doped optical fiber amplifiers and lasers (Shi 1996; Dejneka et al. 2002; Polynkin et al. 2004; Cheng and Xiao 2005). The development of Er-doped silica planar waveguide amplifiers has also been investigated (Poulsen et al. 2003; Bulla et al. 2005; Armelao et al. 2005) to be applied in integrated optical systems. As integrated optical amplifiers should be as short as possible (a few centimeters), a large amount of rare-earth concentration is required than in Er-doped fiber amplifiers (EDFAs). However, due to the onset of concentration quenching at low doping level in silica hosts, the relatively low gains/unit length which can be achieved has made such development difficult. Consequently, silica is an unsuitable host in small and compact amplifiers due to low solubility for erbium.

Thus, there is an interest to obtain different hosts with high solubility for rare-earth elements, especially erbium. One of the potential host candidate is yttrium aluminum borate ($YAl_3(BO_3)_4$, YAB), where yttrium can be substituted by erbium, because Y^{3+} ionic radii (0.090 nm) is very close that of the Er^{3+} (0.089 nm) (Lide 2003). The YAB composition possesses many good properties as a host material for solid state laser such as high physical and chemical stability, high thermal conductivity, good mechanical strength (Liao et al. 2004) and, on the other hand, YAB crystals exhibit a rather high nonlinear optical coefficient (Filimonov et al. 1974).

There is also a great interest to obtain amorphous thin films to be applied as waveguides because, in contrast to polycrystalline thin films, there are no grain boundaries which cause a high optical loss. For this purpose the YAB composition is useful because it exhibits a good rare-earth dispersion through yttrium, a high glass transition temperature (higher to 700 °C), and a high refractive index ($n = 1.6$–1.8) in comparison with silica ($n = 1.45$). Furthermore, recently, transparent ceramics have been used as laser medium and became an attractive alternative to single crystal material due to its easy manufacture and low cost (Qin et al. 2004; Kumar et al. 2006; Ikesue and Aung 2006). On the other hand, there has been recent interest in the development of Er-doped solid-state lasers (Qin et al. 2004). Consequently, erbium-doped YAB hosts are promising materials for 1.5 μm-band integrated amplifiers and lasers.

Different methods such as plasma enhanced chemical vapor deposition (PECVD) (Cantore et al. 2004), flame hydrolysis deposition (Wu et al. 2004), liquid phase epitaxy (Romayuk et al. 2006), ion exchange (Liu and Pun 2004), molecular beam epitaxy (Dekker et al. 2004), or sol–gel method (Jenouvrier et al. 2004; Ghosh et al. 2005; Zhu et al. 2005) have already been used with success in the deposition of high quality thin films with optical properties (Cantore et al. 2004; Wu et al. 2004; Romayuk et al. 2006; Liu and Pun 2004). Compared to these methods, the chemical route such as the polymeric precursor method also knows as Pechini method (Neves et al. 2004)) represents a promising low cost deposition method to obtain good planar waveguides. The main advantages of this method compared to the previous ones are the high control of chemical purity, the low temperature of synthesis, the easy incorporation of rare earth ions, and the possibility to cover large substrates by dip-coating and spin-coating techniques. Likewise, the polymeric precursor method appears to be quite attractive for the preparation of multi-component systems since the use of different components at a molecular level can be easily achieved in solutions, not requiring controlled atmosphere (Maia et al. 2004b). On the other hand, the main disadvantage of this method is the fact that resin, from which the thin film is obtained, contains a high amount of organic materials which is incorporated during the polymerization process. Thus, a thermal treatment around 600 °C, under oxygen atmosphere, must be used to remove the organic constituents.

This work concerns the application of the polymeric precursor method to obtain homogeneous $Y_{0.9}Er_{0.1}Al_3(BO_3)_4$ (Er:YAB) ceramic powders and amorphous cracks- and porosity-free thin films at relatively low temperature. The most probable chemical reactions that occur during the synthesis and the thermal decomposition process are proposed. Structural and micro-structural characterizations of the powders and the thin film samples were performed and will be discussed.

Experimental procedure

Synthesis of the resin

The powders and thin films prepared on this study have the composition of $Y_{0.9}Er_{0.1}Al_3(BO_3)_4$. The synthesis of the resin by the polymeric precursor method was achieved using erbium citrate which was formed by dissolving erbium nitrate (Aldrich, 99.9% purity) in an aqueous solution of citric acid (Aldrich, 99.5% purity) at 70–80 °C during 15 min. After homogenizing, yttrium nitrate (Aldrich, 99.9% purity) was added to the Er-citrate solution, and aluminum nitrate (Prolabo, 98% purity) was added to the Y-Er-citrates. After further homogenization (30 min.), D-sorbitol (Aldrich, 99.5% purity) and boric acid (Carlo Erba, 99.8% purity) were dissolved in water during 1 h and added to the citrate solution. D-sorbitol instead of ethylene glycol, commonly used as polymerization agent, was added to promote the polymerization by a polyesterification reaction at around 120 °C, producing a better complexation of

boron within the polymeric clusters (Neves et al. 2004; Maia et al. 2004a). The molar ratio of citric acid to elements (metals + boron) was 3:1. The citric acid/D-sorbitol mass ratio was set to 3:2.

Powder preparation and characterization techniques

In order to obtain homogeneous powders, firstly, the resins were dried at 80 °C during 1 day, followed by a calcination at 400 °C and 700 °C during 24 h and a heat treatment at 1,150 °C to complete the crystallization of the (Y,Er)AB desired. O_2-rich atmosphere and a heating ratio of 1–20 °C/min were used during the heat treatments. According to literature, 1,150 °C is the best temperature to crystallize the YAB phase (ICDD 1998, JCPDS no. 18-0022).

The weight loss of dried resin powder over a temperature range of 30–800 °C was monitored by thermogravimetric analysis (TGA) in a thermobalance (Netzsch, TASC414/3 controller and TG209 cell) under an oxygen atmosphere and with a heating rate of 2 °C/min. Differential scanning calorimetry (DSC, Netzsch 404 S) was used to study the decomposition reactions of the resin as well as the crystallization of the powders (pre-calcined at 400 °C/24 h and 700 °C/24 h) under O_2 atmosphere with a heating rate of 1, 2, 5, 10, and 20 °C/min over a temperature range of 50–1,000 °C. X-ray diffraction (XRD) analyses were performed in transmission geometry on a Siemens D5000 equipped with a nickel filter and a graphite-diffracted beam monochromator, Cu K_α wavelength ($\lambda = 1.5406$ Å), operating at 40 kV and 50 mA. The XRD patterns were measured on the step scan mode with steps of $2\theta = 0.016°$ and a counting time of 0.65 s per point. The morphology of the powder particles was observed using a high-resolution scanning electron microscope (FEG-VP) (Supra 35, Zeiss, Germany), operating at 3 kV.

Thin film deposition and characterization techniques

Before thin films deposition, the substrates were cleaned with a detergent (Argos, biodegradable anionic surfactant), rinsed with deionized water and placed into an $HNO_3 + HCl$ (16 HNO_3 + 28 HCl + 56 H_2O in mol) solution during 5 min. The substrates were then rinsed once again by deionized water, ethyl alcohol and dried with anhydrous air.

The viscosity of resin used to obtain the thin films was adjusted between 10–30 mPa s by evaporation or by the addition of water. The thin films were deposited on silica substrates by using the spin-coating technique. A spin-coater (RC8 SussMicrotech^{TM}) with the gyrset technology was used in order to improve the thin film uniformity. Rotation acceleration, rotation speed and spin time were fixed at 500 rpm/s, 2,500 rpm, and 5 s, respectively. After the deposition of one layer, the film was dried at 80 °C for 30 min, followed by two intermediary annealing treatments in an O_2 atmosphere at 400 °C during 2 h with a heating rate of 1 °C/min and at 700 °C during 2 h using a 2 °C/min heating-rate. This procedure was repeated for each layer (until nine layers), and finally the film was annealed between 740 and 820 °C during 2 h with a heating rate of 1 °C/min.

The chemical composition of thin films were analyzed by using a scanning electron microscopy (JEOL 840A) equipped with chemical micro-analyzer energy dispersive X-ray (EDX), operating at 10–35 kV, with tungsten electron emitter and secondary electron detection of samples coated by carbon. Grazing incidence X-ray diffraction (GIXRD) measurements of thin films were performed in a home made diffractometer using a PSD (position-sensitive detector) from Inel. Fe K_α ($\lambda = 1.936$ Å) radiation (34 KV/25 mA), a divergence slit of 2 mm, a reception slit equal to 0.6 mm and a plane graphite monochromator were used during the measurements. The incident angle of X-ray beam was fixed at 0.3°, 0.5° or 1°. The scan range (2θ) was 12–90°; simultaneous scans each 1 s. The total time of a GIXRD pattern measurement was 7,200 s. The microstructure of thin films was analyzed using a high-resolution scanning electron microscope (FEG-VP Supra 35, Zeiss, Germany). The surface morphology of the films was analyzed by using an atomic force microscope (AFM-Digital instrument's Nanoscope III) in the tapping mode to measure the surface roughness and the grain size. The thickness of each layer (previously dried at 80 °C/20 min, partially removed by means of a scalpel, and heat-treated at 780 °C for 2 h) was measured by using a perfilometer (Dektak 32, Veeco).

Results and discussion

Firstly, the decomposition reactions of dried resins were studied by DSC and TGA techniques. The DSC curves of the resins dried at 80 °C/14 days are shown in Fig. 1a for different heating rates (1, 2, 5, 10, and 20 °C/min). The pyrolysis and the combustion reactions start around 200 °C and finish between 455 °C f and 687 °C depending on the heating rates used in these DSC experiments. With the increasing the heating rate, the exothermic peaks become more intense and some reactions could be separately detected using 20 °C/min. These peaks are interpreted as resulting from three main reactions: firstly, polymer dehydration (–OH groups) (peak around 362 °C) and nitrate (NO_x) elimination (intense peak at 375 °C); secondly, carbon oxidation and breakdown of carbon–carbon bonds and its elimination in the form of CO_2 and H_2O (broad peak centered at 480 °C); and finally, breakdown of carbon-oxygen-cation and carbon-cation bonds and its oxidation, followed by CO_2 elimination (broad peak centered at 549 °C).

Figure 1b shows in more details the same DSC curves between 650 °C and 1,000 °C. One can observe a very small crystallization peak (T_c) that appears at 813 °C using 1 °C/min. This crystallization peak become more intense and moves typically to higher temperatures as the heating rate increases. It occurs due to the shorter reaction time caused by a higher heating rate, the thermal delay increases accordingly and because of the latent heat the exothermic peak grows. At higher heating rates (10 and 20 °C/min), we observed three additional crystallization peaks between 830 and 970 °C (Fig. 1b). These peaks were determined by coupled DSC/XRD measurements and it is in good agreement with published works (Madarász et al. 2001; Beregi et al. 2000). The first one at ~845 °C is mainly due to $Al_4B_2O_9$ crystallization whereas the second one, centered at ~910 °C, is due to crystallization of (Er, Y)BO_3 phase. The peak centered at ~935 °C is due to crystallization of (Y, Er)$Al_3(BO_3)_4$ and (Y, Er)$Al_2B_4O_{10.5}$ phases. X-ray diffraction measurements of powder sample heat-treated at 1,000 °C (not presented here), reveal the presence of three phases: (Y, Er)$Al_3(BO_3)_4$, (Y, Er)BO_3, (Y, Er)$Al_2B_4O_{10.5}$, being (Y, Er)$Al_3(BO_3)_4$ the major phase. According to published works about the Y_2O_3–$3Al_2O_3$–$4B_2O_3$ system (Madarász et al. 2001; Beregi et al. 2000), the formation of $YAl_3(BO_3)_4$ phase, expected by using a solid-state reaction method, is proceeded and accompanied by the appearance of YBO_3 and $Al_4B_2O_9$ intermediate phases respectively. The different intermediate phases that are observed in our case are related to

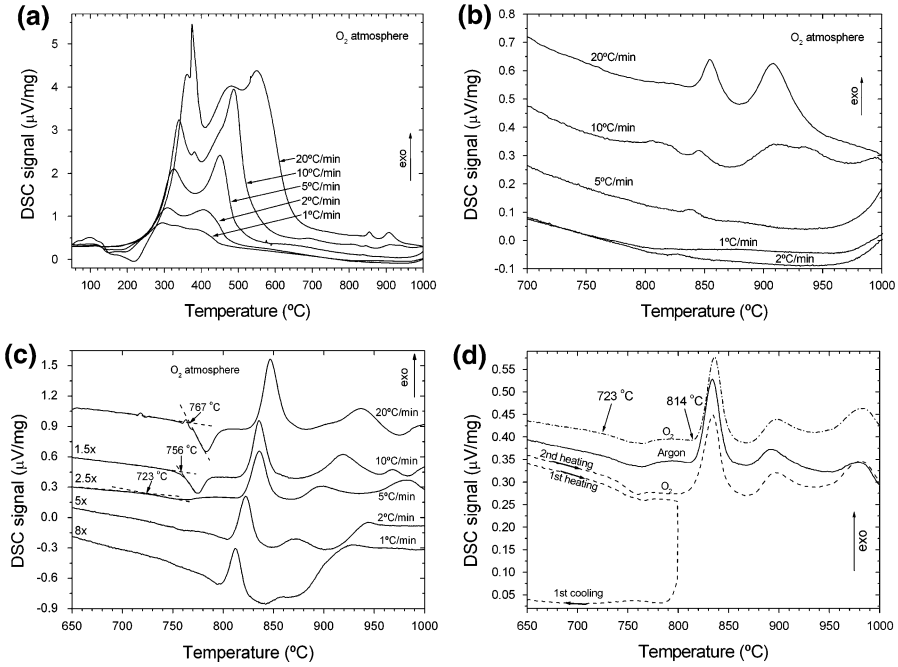

Fig. 1 DSC curves of $Y_{0.9}Er_{0.1}Al_3(BO_3)_4$ (**a**–**b**) resins previously dried at 80 °C/14 days and (**c**) powders previously heat treated at 400 °C and 700 °C/24 h, for different heating rates. The curves in (**d**) refer to measurements under argon- and O_2^- atmosphere using a heating rate of 5 °C/min, performed on these powders previously heat treated at 400 °C and 700 °C/24 h (see text)

the synthesis process employed. The chemical process used in this work is based on the mix of the elements at an atomic level producing nanometric particles. The large surface area of these nanoparticles can contain surface inhomogeneities favoring the formation of different crystalline phases ($(Y,Er)Al_3(BO_3)_4$, $(Y,Er)BO_3$, $(Y,Er)Al_2B_4O_{10.5}$).

These crystallization peaks can be better observed after the elimination of the organic compounds. The resins dried at 80 °C during 14 days were then heat treated at 400 °C during 24 h and at 700 °C during 24 h under O_2-rich atmosphere using a heating rate of 5 °C/min. DSC curves of the resins after such a treatment are shown in Fig. 1c. The above-mentioned crystallization peak is better resolved, moving to higher temperatures with increasing the heating rate, as already pointed out. The onset of an endothermic peak, which was attributed to a glass transition (T_g) of the samples, is observed around 723 °C when the samples were heated at 5 °C/min, around 756 °C for 10 °C/min, and at 767 °C for 20 °C/min. The small changes at 718 °C and at 763 °C on the DSC curve for the powder heated at 20 °C/min (Fig. 1c) are due to current oscillations in the electrical circuit of the furnace.

To the best of our knowledge, this is the first time that a glass transition is observed on powder samples prepared by the polymeric precursor method. To verify if this endothermic peak is really due to a glass transition effect, DSC curves of these samples were measured at a fixed heating rate of 5 °C/min: (1) under O_2-rich atmosphere up to 800 °C, followed by cooling till 100 °C and heated again until 1,000 °C, and (2) under Ar-rich atmosphere from room temperature to 1,000 °C (Fig. 1d). These DSC curves were compared with a previous one also measured at 5 °C/min. We observe that the above-mentioned peak is present when argon as well as oxygen atmospheres were used, proving that this peak is not due to oxidation reactions. Moreover, the process is seen be highly reversible on cooling. Consequently, this endothermic peak is really due to a glass transition thermal effect.

The strong baseline evolution between T_g and T_c can be attributed, according to the literature (Chrysikos et al. 1996; Shelby 1997; Cormier et al. 2006), to the boron anomalies (transformation from BO_4 to BO_3 units) that change strongly the viscosity of the glassy sample thus modifying its specific heat capacity (C_p).

The thermogravimetry (TGA) and its differential (DTG) curves of the resin dried at 80 °C during 24 h are shown in Fig. 2. These also essentially indicate a complete pyrolysis around 500 °C under O_2-rich atmosphere. A total weight loss around 89% occurs between 50 and 550 °C. The weight loss of about 15% observed from 50 to 135 °C is due to adsorbed water not evaporated by drying at 80 °C, while that of about 74% observed from 135 to 550 °C and involving three superposed broad reactions, is due to NO_x and CO_2 elimination during the pyrolysis of the polymeric resin, in agreement with the previous DSC results (Fig. 1a). This result agrees well with the amount of precursors as nitrates, citric acid and D-sorbitol used in the synthesis.

The chelation and polymerization reactions may be written as follows. For chelation:

$$2C_6H_{14}O_6 + H_3BO_3 \rightarrow BC_{12}H_{27}O_{13} + 2H_2O \quad (1)$$

$$3C_6H_8O_7 \cdot H_2O + M(NO_3)_3 \cdot xH_2O \rightarrow MC_{18}H_{21}O_{21} + 3HNO_3 + (x+3)H_2O \quad (2)$$

where M is Al, Y or Er, and x is equal to 9 for Al, 6 for Y, and 5 for Er; and B is boron.

For polymerization, we will have:

$$BC_{12}H_{27}O_{13} + MC_{18}H_{21}O_{21} \rightarrow MBC_{30}H_{46}O_{33} + H_2O \quad (3)$$

The probable complex product of reaction (3) is structurally $(HOCH_2(CHOH)_3CHOHCH_2O)(HO)B(OCH_2(CHOH)_3CHOHCH_2OCOCH_2C(OH)(COOH)CH_2COO^-)M^{3+}[O^-COCH_2C(OH)(COOH)CH_2COOH]_2$, and this reaction (3) occurs successively forming more

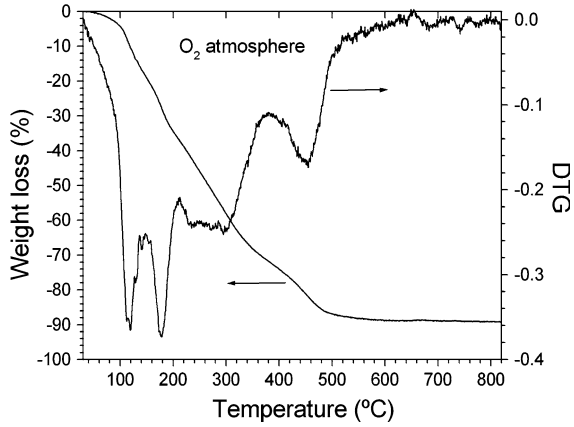

Fig. 2 TGA and DTG curves of $Y_{0.9}Er_{0.1}Al_3(BO_3)_4$ resins previously dried at 80 °C/1 day. Measurements using a 2 °C/min heating rate under O_2 atmosphere

water and polyester, being a tri-dimensional polymer network with B and metallic cation (M) within the complexes. Consequently, we should have a resin with the composition (reduced formula):

$$4MBC_{30}H_{46}O_{33} + nH_2O + 12HNO_3 \quad (4)$$

where M is equal to 0.75Al + 0.225Y + 0.025Er, n is superior to 34, because H_2O was added to dissolve the precursors and chelation/polymerization agents.

Drying the resin at 80 °C, water is partially removed. The suggested reactions occurring during the thermal decomposition of the $Y_{0.9}Er_{0.1}Al_3(BO_3)_4$ resin are summarized below, according to DSC and TGA results, for a heating rate of 2 °C/min:

– Drying from 50 to 135 °C:

$$4MBC_{30}H_{46}O_{33} + nH_2O\uparrow + 12HNO_3 \rightarrow 4MBC_{30}H_{46}O_{33} + 12HNO_3 \quad (5)$$

– Heating the dried resin, structural H_2O, and HNO_3 are eliminated between 135 and 200 °C:

$$4MBC_{30}H_{46}O_{33} + 12HNO_3 \rightarrow 4MBC_{30}H_{28}O_{24} + 36H_2O\uparrow + 12HNO_3\uparrow \rightarrow 4MBC_{30}H_{28}O_{24} \quad (6)$$

– Between 200 and 550 °C, the pyrolysis, oxidation, and combustion reactions occur:

$$4MBC_{30}H_{28}O_{24} + 106O_2 \text{ (from atmosphere)} \rightarrow Y_{0.9}Er_{0.1}Al_3(BO_3)_4 \text{ (amorphous)} + 56H_2O\uparrow + 120CO_2\uparrow \quad (7)$$

The synthesis of organic-free and amorphous nanoparticles is achieved around 600 °C, the amorphous nanoparticles becoming dense at about 780 °C (between T_g and T_c).

$Y_{0.9}Er_{0.1}Al_3(BO_3)_4$ crystalline powder

All the results presented in this section concerns the powdered samples that were previously heat treated at 400 °C and at 700 °C during 24 h. The XRD patterns of the $Y_{0.9}Er_{0.1}Al_3(BO_3)_4$ powders heat treated at 800 °C and at 1,150 °C are shown in Fig. 3. The powder heat-treated at 800 °C is amorphous, in agreement with the previous DSC results

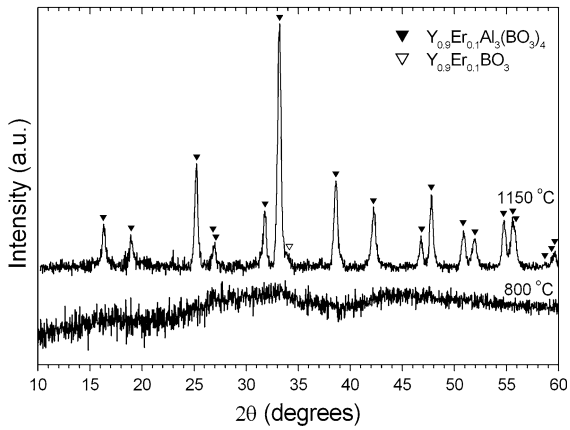

Fig. 3 XRD patterns of amorphous (800 °C) and crystalline (1,150 °C) $Y_{0.9}Er_{0.1}Al_3(BO_3)_4$ nanoparticles

(Fig. 1). The sample annealed at 1,150 °C shows mainly diffraction peaks of $Y_{0.9}Er_{0.1}Al_3(BO_3)_4$ phase and one very weak peak of lower intensity which were attributed to the $Y_{0.9}Er_{0.1}BO_3$ phase. The presence of a small amount of $Y_{0.9}Er_{0.1}BO_3$ phase could arise either due to stoichiometric imbalance (boron loss, mainly) or the lower reaction rate of aluminum oxide with yttrium and boron oxide.

According to previous works (Madarász et al. 2001; Beregi et al. 2000), the solid state reaction of Y_2O_3–$3Al_2O_3$–$4B_2O_3$ compounds leads to the formation of $YAl_3(BO_3)_4$ phase proceeded and accompanied by the crystallization of YBO_3 and $Al_4B_2O_9$ as intermediate phases. Thus, we can consider our method very effective to obtain the $Y_{0.9}Er_{0.1}Al_3(BO_3)_4$ phase when compared to those previous works.

The diffraction peaks and their intensities of the $Y_{0.9}Er_{0.1}Al_3(BO_3)_4$ phase are compared on Table 1 with those of $ErAl_3(BO_3)_4$ (EAB) and $YAl_3(BO_3)_4$ (YAB) crystalline phases. As it can be seen, the diffraction peaks of the $Y_{0.9}Er_{0.1}Al_3(BO_3)_4$ phase occur at lower Bragg angles when compared to pure EAB and YAB phases (ICDD 1998, JCPDS no. 18-0022; ICDD 1998, JCPDS no. 72-1978). This difference can be related to the distortion of the YAB unit cell due to substitution of Y^{3+} atoms by Er^{3+} atoms that have a lower ionic radius (Lide 2003).

Figure 4 shows the evolution of the (202) XRD peak of $Y_{0.9}Er_{0.1}Al_3(BO_3)_4$ powders heat treated at 1,150 °C with different heating rates. We can observe an increase of the degree of crystallinity as the heating rate increases, mainly from 1 to 5 °C/min.

Table 1 Comparison between our X-ray diffraction results for $Y_{0.9}Er_{0.1}Al_3(BO_3)_4$ and the results of other works for $ErAl_3(BO_3)_4$ and $YAl_3(BO_3)_4$

Hkl	$ErAl_3(BO_3)_4$ JCPDS no. 18-0022		$YAl_3(BO_3)_4$ JCPDS no. 72-1978		$Y_{0.9}Er_{0.1}Al_3(BO_3)_4$ This work	
	2θ	Intensity	2θ	Intensity	2θ	Intensity
101	16.556	60	16.450	70.2	16.339	19.6
110	19.237	40	19.081	26.6	18.986	15
021	25.420	60	25.294	44.4	25.195	42.6
012	27.047	40	26.975	28.7	26.921	11.6
211	31.971	60	31.877	42.1	31.792	23.2
202	–	–	33.252	99.9	33.184	100
300	33.407	100	33.365	68.2	–	–
003	–	–	37.210	1.4	37.204	2.4
122	–	–	38.618	23.8	38.603	36.6
220	38.765	80	38.717	31	39.114	4.4
113	42.214	60	42.142	15.5	42.237	13
131	42.422	60	42.328	27.5	42.237	13
401	46.916	40	46.814	14.3	46.786	12.9
312	47.887	40	47.821	26.9	47.783	28.9
033	–	–	50.832	11.3	50.853	7.8
321	51.037	40	50.992	15.3	50.853	7.8
104	51.720	30	51.701	1.8	51.946	4.7
042	–	–	51.938	12.2	51.946	4.7
410	52.132	40	52.018	15	51.946	4.7
223	54.864	60	54.784	24.1	54.744	18.2
024	55.658	40	55.610	21.7	55.628	9.4
232	55.953	40	55.836	13.3	55.628	9.4
051	58.804	20	58.698	3	–	–
214	59.429	30	59.344	6.7	59.567	3.7
330	59.767	10	59.633	7.2	59.567	3.7

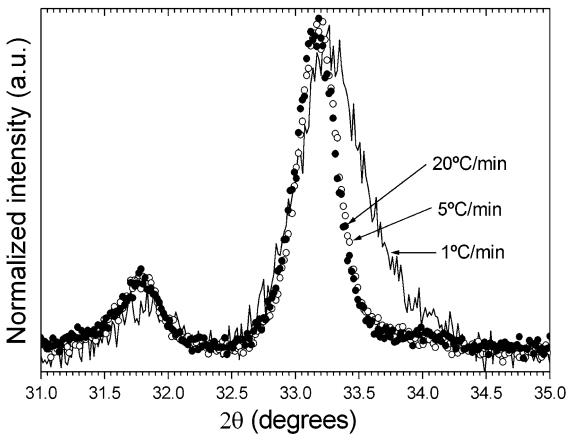

Fig. 4 XRD patterns of crystalline (1,150 °C) $Y_{0.9}Er_{0.1}Al_3(BO_3)_4$ nanoparticles for different heating rates

The microstructures of the powder sample were also studied by FEG. Figure 5a shows the micrograph of the sample heat treated at 400 °C and at 700 °C during 24 h while Fig. 5b refers to the sample heat treated at 1,150 °C. In both cases, a high-coalescence of the nanometric particles is observed. The micrograph (a) also indicates a significant powder densification, with a partial content of liquid phase (△) because the sample was heat treated below but close to T_g. Significative microstructural changes are observed above T_g. The micrograph (b) shows coalesced grains with size around 200 nm forming well-densified plate-like particles.

In summary, using the polymeric precursor method we could prepare a nanometer sized powder sample of Er:YAB phase without the presence of

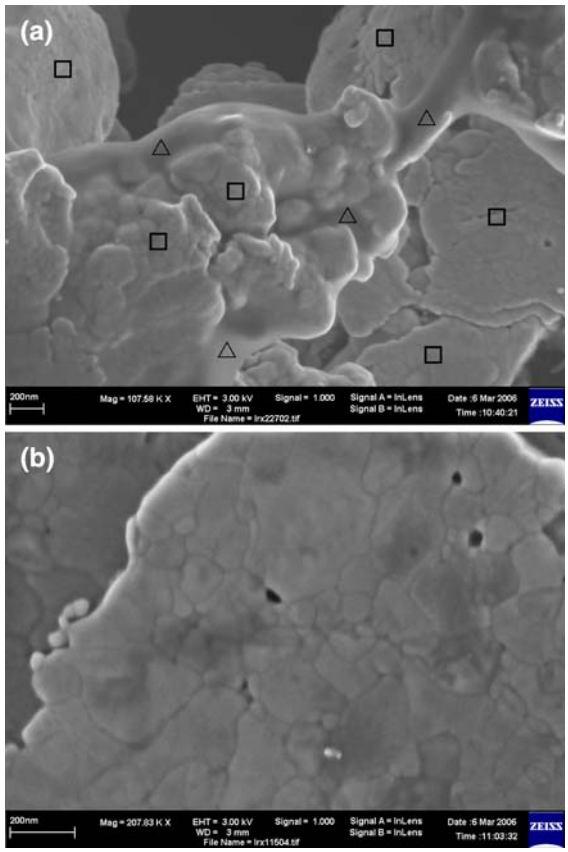

Fig. 5 FEG images of (**a**) amorphous (800 °C), and (**b**) crystalline (1,150 °C) $Y_{0.9}Er_{0.1}Al_3(BO_3)_4$ nanoparticles. □ are amorphous regions from the precursor powder and △ are liquid phase due to T_g

secondary phases. This is thus a promising method to prepare bulk ceramics.

$Y_{0.9}Er_{0.1}Al_3(BO_3)_4$ amorphous thin films

The thin films were obtained from solutions with different viscosity, on silica substrates using the spin-coating technique. Rotation acceleration, rotation speed and spinning time were fixed at 500 rpm/s, 2,500 rpm, and 5 s, respectively. The coatings were annealed in an O_2 atmosphere at 400 °C during 2 h with a heating rate of 1 °C/min and at 700 °C during 2 h using a 2 °C/min heating rate, and then annealed just above T_g, between 740 and 820 °C during 2 h with a heating rate of 1 °C/min.

The EDX technique was used to evaluate the thin films composition heat-treated at 700 °C/2 h and the experimental composition is shown in the Table 2. The experimental values are very close to the nominal composition showing good agreement for all elements measured. The boron content was not measured due to low detection efficiency of this element

The sols show interesting properties for the preparation of dense and crack-free transparent $Y_{0.9}Er_{0.1}Al_3(BO_3)_4$ coatings. The surface morphology of the films sintered at 740 °C for 2 h is shown in Fig. 6a and b. The images (a) and (b) refers to the FEG and AFM measurements, respectively. The surface of the thin films heat-treated at 740 °C is very smooth with a surface RMS roughness of 0.13 nm. This is corroborated by the glass transition of material measured by DSC and observed by FEG images for the powders previously heat treated at 700 °C/24 h presenting already a liquid phase.

The microstructures characterized by AFM of films prepared from different solution viscosities are presented in Fig. 7. As can be observed, the samples present a homogeneous microstructure. The average grain size and the surface RMS roughness of the films were also estimated using AFM micrographs. Figure 8a shows the RMS roughness and grain size values as a function of viscosity of the initial solution (sol). Treatments at 780 °C of thin films deposited using solutions with different viscosities led to grain growth and to an increase of the surface RMS roughness. This effect is related to crystallization and to more condensed polymeric clusters in more viscous precursor solutions that reduce the flow off during the spinning. From the same effect, the thickness has a linear increase as a function of the viscosity (Fig. 8b). Thickness were measured using a perfilometer.

GIXRD patterns of $Y_{0.9}Er_{0.1}Al_3(BO_3)_4$ thin film annealed during 2 h at 740, 780, and 820 °C are presented in Fig. 9. As can be seen, the films are

Table 2 EDX analysis results of $Y_{0.9}Er_{0.1}Al_3(BO_3)_4$ thin film for Y, Er, and Al elements

Elements	Composition	
	Experimental	Nominal
Y	0.220 ± 0.005	0.225
Er	0.024 ± 0.002	0.025
Al	0.756 ± 0.005	0.750

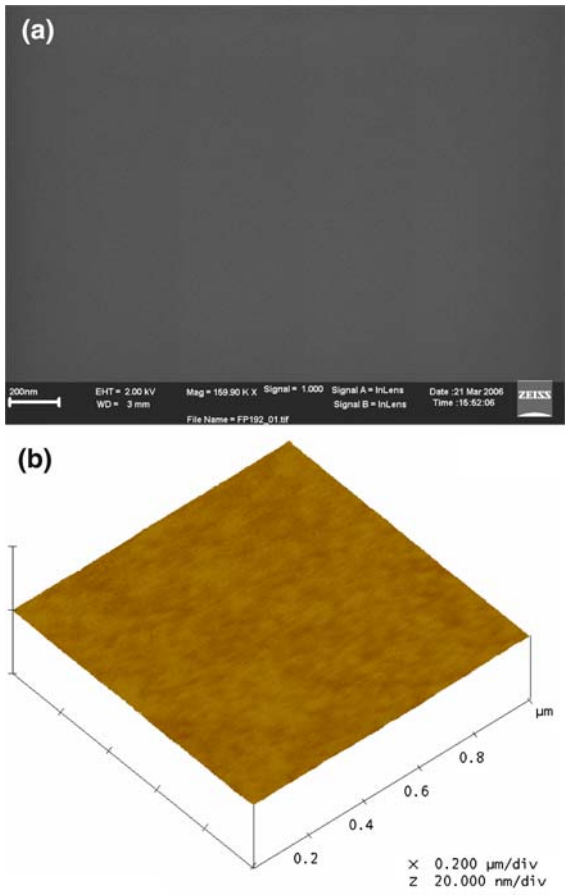

Fig. 6 (**a**) FEG and (**b**) AFM images of $Y_{0.9}Er_{0.1}Al_3(BO_3)_4$ thin films sintered at 740 °C for 2 h for 25 mPa s viscosity solution

amorphous until the sintering temperature rises to 780 °C when the first diffraction peaks indexed as those of $Al_4B_2O_9$ crystalline phase are observed. The stability of these films against the crystallization indicates that they can be used on optical applications as waveguides and amplifiers in integrated optical systems.

Thin films which were prepared with a 25 mPa s viscosity solution present an average grain size around 42 ± 2 nm with a high degree of coalescence, a surface RMS roughness around 0.37 nm and a thickness of 76 ± 2 nm. Under this condition, crack- and porosity-free thin films were obtained. Herewith, these films (when heat treated at 740 °C) are useful to be applied as waveguides and amplifiers. The material studied presents properties within requirements previously reported (Uhlmann et al. 1996). That is, for signal processing in the plane of the film

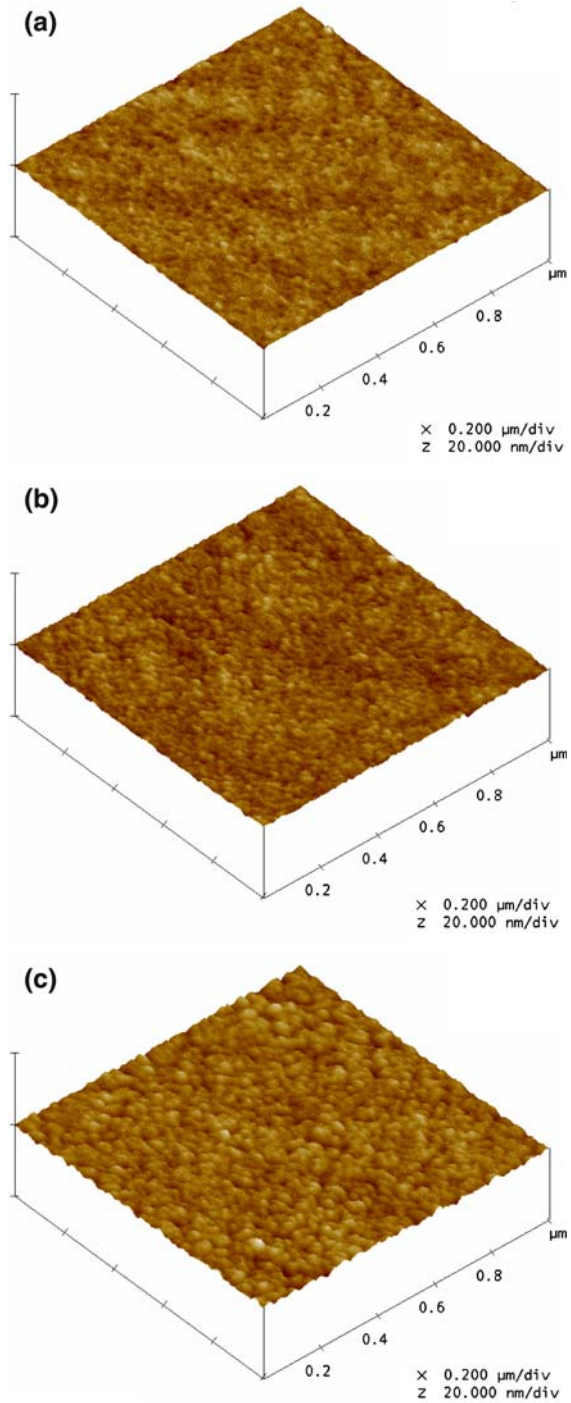

Fig. 7 AFM surface morphology of a $Y_{0.9}Er_{0.1}Al_3(BO_3)_4$ thin film sintered at 780 °C for 2 h for different precursor resin viscosities: (a) 10, (b) 20, and (c) 30 mPa s

(waveguides), inhomogeneities in the refractive index, *n*, must be minimized to reduce attenuation

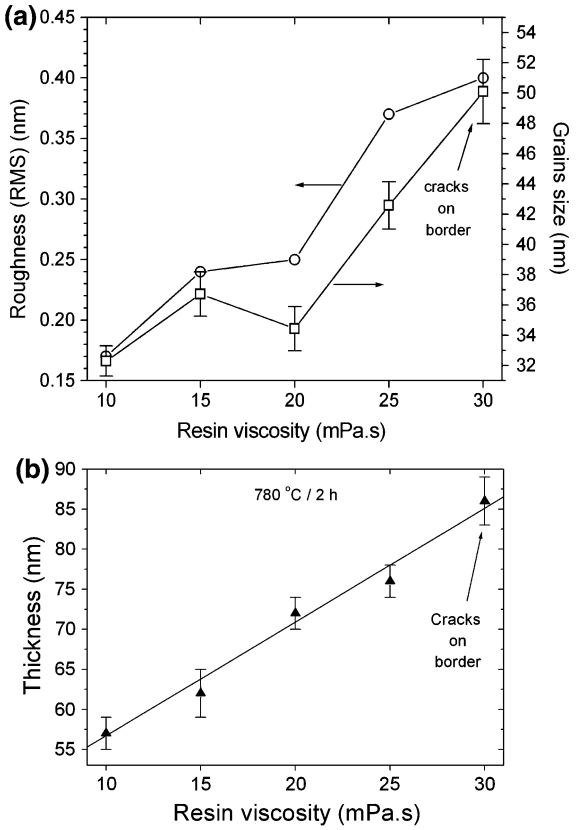

Fig. 8 (a) RMS roughness and grains size, and (b) thickness of the $Y_{0.9}Er_{0.1}Al_3(BO_3)_4$ thin films sintered at 780 °C during 2 h for different precursor resin viscosities

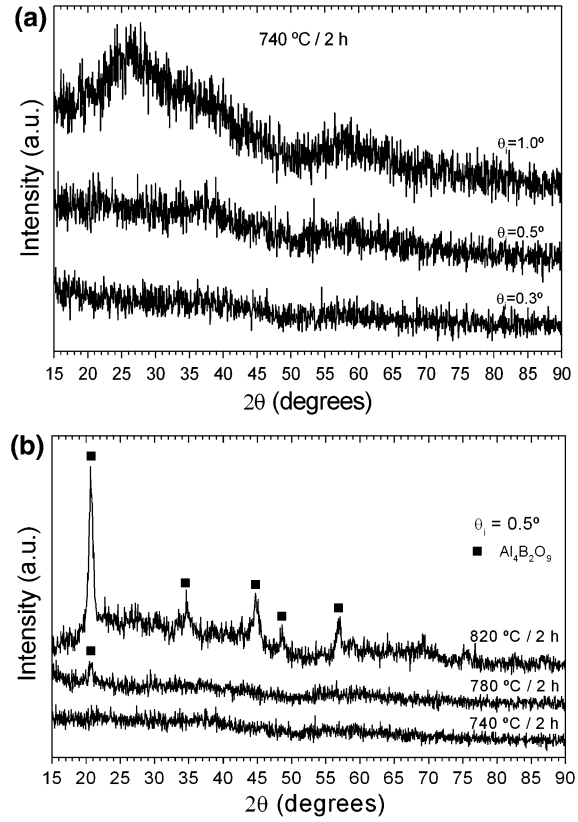

Fig. 9 GIXRD patterns of amorphous (740 °C) and partially crystallized (820 °C) $Y_{0.9}Er_{0.1}Al_3(BO_3)_4$ thin films. (**a**) Patterns of $Y_{0.9}Er_{0.1}Al_3(BO_3)_4$ amorphous thin film for different incidence angles. (**b**) Measurements of $Y_{0.9}Er_{0.1}Al_3(BO_3)_4$ thin films for different heat treatments

losses; this reduction can be achieved with either amorphous or single crystal materials, because grain boundaries in polycrystalline materials are regions of compositional or structural discontinuity which produce undesirable variations in n. However, this requirement does not preclude the use of oriented epitaxial films. As the $Y_{0.9}Er_{0.1}Al_3(BO_3)_4$ material studied crystallizes on a single phase only at high temperature (1,150 °C), then the crystalline form become useless. Thus, $Y_{0.9}Er_{0.1}Al_3(BO_3)_4$ is very promising to be used in amorphous state (when heat treated at about 740 °C) as waveguides and compact planar optical amplifiers.

Conclusions

$Y_{0.9}Er_{0.1}Al_3(BO_3)_4$ crystalline powders and amorphous thin films were successfully prepared using a modified polymeric precursor method in which D-sorbitol is used to replace ethylene glycol in order to improve better boron complexation into the polymerized framework. The chemical reactions of complexation, polymerization and resin decomposition were described, corroborating with DSC and TGA results. $Y_{0.9}Er_{0.1}Al_3(BO_3)_4$ powders heat treated at 800 °C were amorphous in agreement with the DSC results, and $Y_{0.9}Er_{0.1}Al_3(BO_3)_4$ crystallizes as main phase at 1,150 °C, with a very small amount of $Y_{0.9}Er_{0.1}BO_3$, probably due to stoichiometric imbalance (small boron loss) at high temperatures. This synthesis of $Y_{0.9}Er_{0.1}Al_3(BO_3)_4$ powder is thus promising for the preparation of bulk ceramics. On the other hand, this process is also interesting for the preparation of optical glassy waveguides, due to its high difference between the glass transition and crystallization temperatures (around 90 °C), showing good thermal stability. X-ray diffraction shows that

only after 2 h at 780 °C the crystallization process occurs. Heat treatment of precursor films at 740 °C is most recommended to prepare high-quality amorphous $Y_{0.9}Er_{0.1}Al_3(BO_3)_4$ films (multi-layers until 800 nm) to be applied as waveguides and optical amplifiers free of cracks and pores, with very smooth and dense surface. High quality thin films were prepared without any macroscopic defect. In this work heat-treatment and thickness were adjusted to prepare homogeneous, dense and glassy thin films. Multilayer thin films preparations are in progress to perform then their optical characterizations.

Acknowledgments This work was supported by Brazilian research-funding agencies, FAPESP (No. 02/13748-9) and CAPES (No. 455/04-1). The authors would like to thank Dr Nathalie Sanz for AFM measurements and valuable discussions.

References

Armelao L, Gross S, Obetti G, Tondello E (2005) Er^{3+}-doped SiO_2-Al_2O_3 thin films prepared by the sol–gel route. Surf Coat Technol 190:218–222

Beregi E, Watterich A, Kovács L, Madarász J (2000) Solid-state reactions in Y_2O_3:$3Al_2O_3$:$4B_2O_3$ system studied by FTIR spectroscopy and X-ray diffraction. Vib Spectrosc 22:169–173

Bulla DAP, Li WT, Charles C, Boswell R, Ankiewicz A, Love JD (2005) Low-loss silica-based optical film waveguides deposited by helicon-activated reactive evaporation. J Lightwave Technol 23:1302–1307

Cantore F, Della Corte FG, Nigro MA, Summonte C (2004) In-guide measurement of the infrared absorption variation induced in hydrogenated amorphous silicon by visible radiation. J Non-Cryst Solids 338:249–253

Cheng C, Xiao M (2005) Optimization of an erbium-doped fiber amplifier with radial effects. Opt Commun 254:215–222

Chryssikos GD, Kamitsos EI, Yiannopoulos YD (1996) Towards a structural interpretation of fragility and decoupling trends in borate systems. J Non-Cryst Solids 196:244–248

Cormier L, Majerus O, Neuville DR, Calas G (2006) Temperature-induced structural modifications between alkali borate glasses and melts. J Am Ceram Soc 89:13–19

Dejneka MJ, Hanson BZ, Crigler SG, Zenteno LA, Minelly JD, Allan DC, Miller WJ, Kuksenkov D (2002) La_2O_3-Al_2O_3-SiO_2 glasses for high-power, Yb^{3+}-doped, 980-nm fiber lasers. J Am Ceram Soc 85:1100–1106

Dekker R, Klunder DJW, Borreman A, Diemeer MBJ, Worhoff K, Driessen A, Stouwdam JW, van Veggel FCJM (2004) Stimulated emission and optical gain in LaF_3:Nd nanoparticle-doped polymer-based waveguides. Appl Phys Lett 85:6104–6106

Filimonov AA, Leonyuk NI, Meissner LB, Timchenko TI, Rez IS (1974) Nonlinear optical properties of isomorphic family of crystals with yttrium-aluminium borate (YAB) structure. Krist Tech 9:63–66

Ghosh PK, Das S, Chattopadhyay KK (2005) Temperature dependent structural and optical properties of nanocrystalline CdO thin films deposited by sol–gel process. J Nanopart Res 7:219–225

Ikesue A, Aung YL (2006) Synthesis and performance of advanced ceramic lasers. J Am Ceram Soc 89:1936–1944

International Centre for Diffraction Data (ICDD) (1998) JCPDS no. 18-0022–$ErAl_3(BO_3)_4$

International Centre for Diffraction Data (ICDD) (1998) JCPDS no. 72-1978–$YAl_3(BO_3)_4$

Jenouvrier P, Fick J, Audier M, Langlet M (2004) Microstructure and photoluminescence properties of sol–gel $Y^{-}{}_2$xErxTi_2O_7 thin films. Opt Mater 27:131–137

Kik PG, Polman A (1998) Erbium doped optical-waveguide amplifiers on silicon. MRS Bull 23:48–54

Kumar GA, Lu JR, Kaminskii AA, Ueda KI, Yagi H, Yanagitani J (2006) Spectroscopic and stimulated emission characteristics of Nd^{3+} in transparent Y_2O_3 ceramics. IEEE J Quantum Electron 42:643–650

Liao J, Lin Y, Chen Y, Luo Z, Huang Y (2004) Flux growth and spectral properties of Yb:YAB single crystal with high Yb^{3+} concentration. J Cryst Growth 267:134–139

Lide DR (2003) CRC handbook of chemistry and physics. 84th edn. CRC Press, USA

Liu K, Pun EYB (2004) K^{+}-Na^{+} ion-exchanged waveguides in Er^{3+}-Yb^{3+} codoped phosphate glasses using field-assisted annealing. Appl Opt 43:3179–3184

Madarász J, Beregi E, Sztatisz J, Földvári I, Pokol G (2001) Combined DTA and XRD study of sintering steps towards $YAl_3(BO_3)_4$. J Therm Anal Calorim 64:1059–1065

Maia LJQ, Bernardi MIB, Feitosa CAC, Mastelaro VR, Zanatta AR, Hernandes AC (2004a) Synthesis and characterization of beta barium borate thin films obtained from the BaO-B_2O_3-TiO_2 ternary system. Thin Solid Films 457:246–252

Maia LJQ, Bernardi MIB, Zanatta AR, Hernandes AC, Mastelaro VR (2004b) beta-BaB_2O_4 nanometric powder obtained from the ternary BaO-B_2O_3-TiO_2 system using the polymeric precursor method. Mater Sci Eng B - Solid State Mater Adv Technol 107:33–38

Neves PP, Maia LJQ, Bernardi MIB, Zanatta AR, Mastelaro VR, Zanetti SM, Leite ER (2004) Synthesis and characterization of the beta-BaB_2O_4 phase obtained by the polymeric precursor method. J Sol-Gel Sci Technol 29:89–96

Polynkin O, Temyanko V, Mansuripur M, Peyghambarian N (2004) Efficient and scalable side pumping scheme for short high-power optical fiber lasers and amplifiers. IEEE Photonics Technol Lett 16:2024–2026

Poulsen MR, Borel PI, Fage-Pedersen J, Hubner J, Kristensen M, Povlsen JH, Rottwitt K, Svalgaard M, Svendsen W (2003) Advances in silica-based integrated optics. Opt Eng 42:2821–2834

Qin G, Lu J, Bisson JF, Feng Y, Ueda KI, Yagi H, Yanagitani T (2004) Upconversion luminescence of Er^{3+} in highly transparent YAG ceramics. Solid State Commun 132:103–106

Romanyuk YE, Borca CN, Pollnau M, Rivier S, Petrov V, Griebner U (2006) Yb-doped $KY(WO_4)_2$ planar waveguide laser. Opt Lett 31:53–55

Shelby JE (1997) Introduction to glass science and technology. The Royal Society of Chemistry, Cambridge, UK

Shi CX (1996) A novel single-mode Er-doped fiber-ring laser: experiment. Microwave Opt Technol Lett 11:187–190

Uhlmann DR, Boulton JM, Teowee G (1996) New optical materials by wet chemical processing. J Non-Cryst Solids 196:26–36

Urquhart P (1988) Review of rare-earth doped fiber lasers and amplifiers. IEE Proc - J Optoelectron 135:385–402

Wu YD, Xing H, Zhang LT, Li AW, Zheng W, Liu GF, Guo YB, Zhang YS (2004) Fabrication and properties of vitreous silica films prepared by flame hydrolysis deposition. Mater Chem Phys 84:234–237

Zhu XP, Yukawa T, Kishi T, Hirai M, Suematsu H, Jiang W, Yatsui K (2005) Synthesis of light-emitting silicon nanoparticles by intense pulsed ion-beam evaporation. J Nanopart Res 7:669–673